Supporting Information

Bilokapic and Schwartz 10.1073/pnas.1205151109

SI Materials and Methods

Yeast Strains and Genetic Techniques. The *Schizosaccharomyces pombe* strains used in the study are listed in Table S1. Gene disruption of nucleoporins (or Nups) was carried out in haploid strains by homologous integration of the PCR fragments corresponding to the KanMX6 module. pFA6a-GFP(S65Y)-hph was used as a template for C-terminal GFP tagging (1). Deletion of Nup120 in *S. pombe* leads to a temperature-sensitive phenotype. Therefore, the experiments were performed at the permissive temperature of 25 °C.

pREP1 vector (a gift from D. Moazed, Harvard Medical School, Boston, MA) with flag-tagged Nup120 was used in the experiments to supplement Δ*nup120*. The *nmt1* promoter of pREP1 was replaced with the Nup37 promoter region to obtain a WT nucleoporin expression level, whereas EGFP was subcloned from pIC242 (gift from I. Cheeseman, Whitehead Institute for Biomedical Research, Cambridge, MA) in front of the multiple cloning site, yielding pREP-GFP plasmid.

Yeast Two-Hybrid and FISH Analysis. Genes for components of the human Y-complex were amplified from in-laboratory storage vectors. PCR products were cloned in-frame with the 3′-end of the transcription factor Gal4-activation domain of pACT2 prey vector and/or in-frame with the 3′-end of the transcription factor LexA-DNA binding domain of the bait plasmid pAB151. The constructs were introduced by electroporation into L40 *Saccharomyces cerevisiae* strain (plasmids and yeast strain were gifts from I. Weygand-Durasevic, Faculty of Science, Zagreb, Croatia). Yeast two-hybrid analysis was performed as described by Bilokapic et al. (2). Cy5-labeled 50-mer oligo dT probe was used for poly $(A)^+$RNA FISH assay, and analysis was performed as described by Seo et al. (3).

Expression Plasmid Constructs and Protein Purification. *S. pombe* Nup120 and Nup37 were cloned into a pET-Duet plasmid to yield 6 × His-6 × Arg-SUMO–tagged Nup120 in the first cassette and SUMO-tagged Nup37 in the second cassette. Both tags are cleavable by 3C protease. Proteins were coexpressed in *Escherichia coli* BL21 (DE3) RIL strain. After overnight induction at 18 °C, cells were resuspended in lysis buffer [50 mM sodium phosphate (pH 8.0), 400 mM NaCl, 40 mM imidazole, 3 mM β-mercaptoethanol, 1 mM PMSF]. The protein complex was Ni-affinity purified and dialyzed at 4 °C [20 mM Hepes·KOH (pH 7.5), 150 mM NaCl, 0.1 mM EDTA, 1 mM DTT] before further purification via cation-exchange chromatography. The tags were proteolytically removed, and the sample was loaded onto Superdex S200 16/60 column (GE Healthcare) equilibrated in crystallization buffer [10 mM Hepes·KOH (pH 7.5), 150 mM NaCl, 1 mM DTT]. Nup120 and Nup37 mutants were separately expressed in *E. coli* and purified as described above. Selenomethionine (SeMet)-labeled complex was prepared as described (4). Protein purification was carried out as for the native complex.

Cells expressing 6 × His-6 × Arg-SUMO–tagged *S. pombe* $ELY5_{1–272}$ were mixed with cells expressing the Nup120–Nup37 complex. The protein complex was purified via Ni-affinity resin as described using 300 mM NaCl instead of 400 mM NaCl in the lysis buffer and loaded onto a gel-filtration column. Fractions with the protein complex were collected and run again on a gel-filtration column.

Full-length *S. pombe* Nup85 was cloned into a pET-Duet vector encoding 3C-cleavable 6 × His-SUMO tag. Full-length *S. pombe* Seh1 was cloned into a pGEX-4T1 vector, with 3C-cleavable GST tag. Protein coexpression and Ni-affinity purification were performed as for the Nup120–Nup37 complex. The Nup85–Seh1 complex was further purified on GST-affinity resin. The N-terminal tags were proteolytically removed before a final gel-filtration step.

S. pombe Nup145C (residues 1,089–end) and Sec13 were inserted into modified pET-Duet and pGEX-4T1 vectors, respectively. The same purification protocol was used for Nup145C–Sec13 and Nup85–Seh1 complexes.

S. pombe strains with FLAG-tagged Nup120 were grown at 30 °C to an OD_{600} of ∼1.5. Cells were harvested and washed with the binding buffer [20 mM Hepes·KOH (pH 7.5), 150 mM NaCl, 110 mM K(OAc), 2 mM $MgCl_2$, 1 mM DTT, 1 mM PMSF, protease inhibitor mixture tablets] before freezing in liquid nitrogen. Cells were ground in a freezer mill. The lysate was centrifuged and incubated with FLAG-antibody beads for 2 h at 4 °C. Beads were thoroughly washed with the binding buffer. Bound proteins were eluted from beads by incubation with FLAG peptide in the buffer. Anti-GFP and HP-conjugated anti-mouse secondary antibodies were used for Western blot analysis.

E. coli glutamate dehydrogenase (EcGDH) was purified using Ni-affinity, ion exchange, and size exclusion chromatography.

Protein–Protein Interaction Experiments. Protein interaction experiments were carried out on a Superdex 200 HR 10/300 column equilibrated in gel-filtration buffer [10 mM Hepes·KOH (pH 7.5), 150 mM NaCl, 1 mM DTT].

For Nup85-Seh1-Nup145C-Sec13 tetramer formation, equimolar amounts of purified Nup85–Seh1 and Nup145C–Sec13 complexes were mixed and incubated on ice for 5 min.

Equimolar amounts of Nup120PD (residues 1–545) and Nup120HD (residues 546–1,136) were mixed with 1.5-fold molar excess of WT or mutant Nup37 and incubated for 30 min at room temperature. Control samples were analyzed in the same way.

Binding of full-length Nup120, Nup120 truncations, and Nup120ΔHB (residues 399–515 replaced with a serine-glycine loop) to the Nup85–Seh1–Nup145C–Sec13 complex was performed in gel-filtration buffer supplemented with 10% (vol/vol) glycerol or with 1 mM spermidine and incubated for 30 min on ice. Control samples were analyzed in the same way.

To assess the interactions between GFP-ELY5 and recombinant Nup120 and Nup37 proteins, we prepared Nup37-, Nup120-, and Nup120-Nup37–coated Ni-affinity beads. Washed beads were incubated with *S. pombe* extracts containing GFP-ELY5 for 1.5 h at 4 °C. After repeated washing, proteins were eluted from beads using SDS-sample buffer and resolved by SDS/PAGE. ELY5 was detected using GFP antibodies.

Protein Crystallization. Initial crystals of the Nup120–Nup37 complex were obtained in sitting drops using commercial screens [100 mM Bis-Tris·HCl (pH 5.50), 3 M NaCl] after in-drop limited proteolysis with chymotrypsin. Bigger crystals were obtained with the hanging drop vapor diffusion method in 2 + 2-μL drops, with a protein sample freshly treated with chymotrypsin. The crystals were carefully washed before analysis on the SDS gel. In addition to Nup120 and Nup37, which appeared as undigested full-length proteins on the SDS gel, a third protein was detected. Mass spectrometric analysis confirmed that the additional protein in the crystal is ecGDH. Purity of the Nup120–Nup37 complex was improved by adding a hexaarginine tag at the N terminus of Nup120, enabling an additional ion-exchange purification step. With the modified purification scheme, the Nup120-Nup37 protein sample

was free of any contaminations. To optimize the crystals, separately purified ecGDH was added in different molar ratios. The largest and optically best crystals were obtained by mixing 5 mg/mL pure Nup120–Nup37 complex with ecGDH in a 10:1 molar ratio. Crystals were grown in 1 + 1-μL drops [100 mM Bis-Tris·HCl (pH 5.75–6.5), 1.75–2.25 M NaCl) at 18 °C for 3 d before they were cryoprotected by serial transfer into reservoir solutions supplemented with 100 mM NaCl and increasing amounts of glycerol [5–23% (vol/vol), ∼5% steps]. $[Ta_6Br_{12}]^{2+}$-derivatized crystals were obtained by transferring cryoprotected crystals into a cryosolution supplemented with 200 μM $[Ta_6Br_{12}]^{2+} \times 2Br^-$ and incubating for 2 h. Crystals were back-soaked into cryoprotection solution for 10 min and flash-frozen in liquid nitrogen.

The ecGDH-free Nup120–Nup37 complex was also tested for crystallization using commercial screens and a protein concentration of 10 mg/mL. Thin, long needles were obtained with 5 mg/mL pure complex in 100 mM Hepes (pH 7.5), 200 mM NaCl, 10% (wt/vol) PEG 3350, and 10% (vol/vol) isopropanol at 18 °C. These crystals diffracted to 9 Å and were cryoprotected by serial transfer into reservoir solutions supplemented with increasing amounts of glycerol before flash-freezing in liquid nitrogen.

Several initial crystals of the Nup120ΔC–Nup37 complex were identified using commercial sparse-matrix crystallization screens. Crystals obtained in 10 mM Hepes·NaOH (pH 7.5) and 1.9 M MgOAc, and cryoprotected using ethylene glycol, diffracted to barely 9 Å. Optimization of the cryoprotection protocol (slow, stepwise addition of ethylene glycol to a final concentration of 22.5% with a 2-h equilibration period between each step) finally resulted in crystals that diffracted to 4.4 Å. The SeMet derivative crystallized in the same condition, and the crystals were cryoprotected using the same protocol.

Native and SeMet-derivatized Nup37 crystals were obtained at 30 °C in 100 mM Tris·HCl (pH 7.75–8.25), 4% (vol/vol) 1,4-butanediol, and 400–500 mM Li_2SO_4 using 7 mg/mL protein solution. The crystals were cryoprotected at 30 °C by briefly soaking into reservoir solutions supplemented with additional Li_2SO_4 and 22.5% (vol/vol) ethylene glycol.

The ecGDH crystals obtained in 100 mM Bis-Tris·HCl (pH 6.5), 200 mM NH_4Ac, and 19% (wt/vol) PEG 6000 were cryoprotected by soaking in precipitant solution supplemented with 22.5% (vol/vol) PEG 200.

Data Collection and Structure Determination. Diffraction data for all crystals were collected at 100 K at the Northeastern Collaborative Access Team (NE-CAT) beamlines 24-IDC/-E at the Advanced Photon Source at Argonne National Laboratory.

Datasets were scaled and processed using HKL2000 (5). SHELXC/D/E (6) was used for heavy atom searches, and Phaser (7) was used for molecular replacement (MR) searches.

Nup37 was solved by single-wavelength anomalous dispersion (SAD) using a SeMet derivative, and the final structure was refined to 2.6 Å. The model was built with phenix.autobuild (8) and manually in Coot (9). Refinement was carried out using phenix.refine (8).

The Nup120–Nup37 complex crystallized in the presence of ecGDH. Despite its small fraction of the asymmetrical unit (12%), we found a single solution for one molecule of ecGDH by MR. The correctness of the solution was confirmed by building the crystallographic symmetry equivalents. The ecGDH is positioned on the sixfold axis, such that the hexamer is built up in the same way as seen in the pure ecGDH crystal (Fig. S2*B*). Due to the high solvent content (82%), density modification with Parrot (10, 11) revealed many tubular density elements corresponding to α-helices of Nup120. The initial MR phases were used to position seven Ta_6Br_{12} clusters in a derivatized crystal (Fig. S2*A*). These MR-SAD phases allowed for the positioning of two copies of an *S. pombe* Nup120 model threaded based on the published *S. cerevisiae* Nup120 fragment [Protein Data Bank (PDB) ID codes 3HXR and 3F7F]. In the 7.0-Å native crystals, the Nup120 models improved the phases and, together with NCS averaging, revealed better defined density for the two Nup37 molecules and the remaining Nup120. Superpositioning of the two Nup120 structures in the asymmetrical unit revealed that the NCS breaks after α-helix 22 in the C-terminal domain of Nup120. We reasoned that the flexibly positioned C terminus of Nup120 might be the cause for the modest diffraction of the crystals. A shorter Nup120 construct lacking the C-terminal ∼170-residue flexible part was created. The next model building steps were performed using data obtained from crystals of this shorter fragment.

The Nup120ΔC-Nup37 crystals diffracted to 4.4 Å, and initial phases were obtained by MR with the relevant fraction of the full-length Nup120-Nup37 structure. Se-Met protein was crystallized, and a 5.0-Å dataset was obtained. Positions for 15 of 17 possible selenium sites were determined model-independently. Se-Met and MR phases were combined and density-modified. The resulting electron density map, together with the positional SeMet markers, was of sufficient clarity to place Nup37 unambiguously (Fig. S2*F*) and to assign the Nup120 sequence in the 4.4-Å dataset. The sequence assignment of Nup120 was additionally aided using B-factor sharpening, which revealed side chains for some of the bulky residues. The structure was refined by combining deformable elastic network (DEN)-assisted refinement in the CNS (12) with secondary structure and reference model restraints, grouped B-factor, and translation/libration/screw (TLS) refinement in phenix.refine (8). Model building was carried out with Coot (9). The 4.4-Å structure was placed into the 7.0-Å dataset, further improving phases. In our 7.0-Å structure, the C-terminal ends of both Nup120 molecules in the asymmetrical unit are, together with the ecGDH, the best-ordered part of the molecule. The eight-helix portion unique to the 7.0-Å structure is entirely α-helical, and all individual α-helices were visible in the electron density map. The direction of the α-helices is unambiguously assigned because of the HEAT-repeat character of this segment and because most of the connecting loops are short and visible in the electron density map. The sequence assignment was additionally guided by secondary structure prediction and phylogenetic analysis, although in some parts of this ∼170-residue region, a shift by one helical turn cannot be excluded.

For ecGDH, diffraction data were collected to 2.0 Å. ARP/wARP (13) was used to solve the structure by MR using *Plasmodium falciparum* glutamate dehydrogenase (14) (PDB ID code 2BMA). The ecGDH structure was used as the reference model during refinement of the 7.0-Å structure.

The stereochemical quality of the models was validated by Molprobity (15). Statistical parameters of data collection and refinement are given in Tables S2–S6.

Structure Analysis. Sequence alignments were performed using T-coffee (16) and edited with Jalview (17). Structure figures were created in PyMOL.

1. Bähler J, et al. (1998) Heterologous modules for efficient and versatile PCR-based gene targeting in Schizosaccharomyces pombe. *Yeast* 14:943–951.
2. Bilokapic S, et al. (2009) Idiosyncratic helix-turn-helix motif in Methanosarcina barkeri seryl-tRNA synthetase has a critical architectural role. *J Biol Chem* 284:10706–10713.
3. Seo H-S, et al. (2009) Structural and functional analysis of Nup120 suggests ring formation of the Nup84 complex. *Proc Natl Acad Sci USA* 106:14281–14286.
4. Brohawn SG, Leksa NC, Spear ED, Rajashankar KR, Schwartz TU (2008) Structural evidence for common ancestry of the nuclear pore complex and vesicle coats. *Science* 322:1369–1373.
5. Otwinowski Z, Minor W (1997) Processing of X-ray diffraction data collected in oscillation mode. *Methods Enzymol* 276:307–326.
6. Sheldrick GM (2008) A short history of SHELX. *Acta Crystallogr A* 64(Pt 1):112–122.

7. McCoy AJ, et al. (2007) Phaser crystallographic software. *J Appl Cryst* 40:658–674.
8. Adams PD, et al. (2010) PHENIX: A comprehensive Python-based system for macromolecular structure solution. *Acta Crystallogr D Biol Crystallogr* 66:213–221.
9. Emsley P, Lohkamp B, Scott WG, Cowtan K (2010) Features and development of Coot. *Acta Crystallogr D Biol Crystallogr* 66:486–501.
10. Zhang KY, Cowtan K, Main P (1997) Combining constraints for electron-density modification. *Methods Enzymol* 277:53–64.
11. Collaborative Computational Project, Number 4 (1994) The CCP4 suite: Programs for protein crystallography. *Acta Crystallogr D Biol Crystallogr* 50:760–763.
12. Brünger AT, et al. (1998) Crystallography & NMR system: A new software suite for macromolecular structure determination. *Acta Crystallogr D Biol Crystallogr* 54: 905–921.
13. Langer G, Cohen SX, Lamzin VS, Perrakis A (2008) Automated macromolecular model building for X-ray crystallography using ARP/wARP version 7. *Nat Protoc* 3: 1171–1179.
14. Werner C, Stubbs MT, Krauth-Siegel RL, Klebe G (2005) The crystal structure of Plasmodium falciparum glutamate dehydrogenase, a putative target for novel antimalarial drugs. *J Mol Biol* 349:597–607.
15. Chen VB, et al. (2010) MolProbity: All-atom structure validation for macromolecular crystallography. *Acta Crystallogr D Biol Crystallogr* 66(Pt 1):12–21.
16. Notredame C, Higgins DG, Heringa J (2000) T-Coffee: A novel method for fast and accurate multiple sequence alignment. *J Mol Biol* 302:205–217.
17. Waterhouse AM, Procter JB, Martin DMA, Clamp M, Barton GJ (2009) Jalview Version 2—A multiple sequence alignment editor and analysis workbench. *Bioinformatics* 25: 1189–1191.

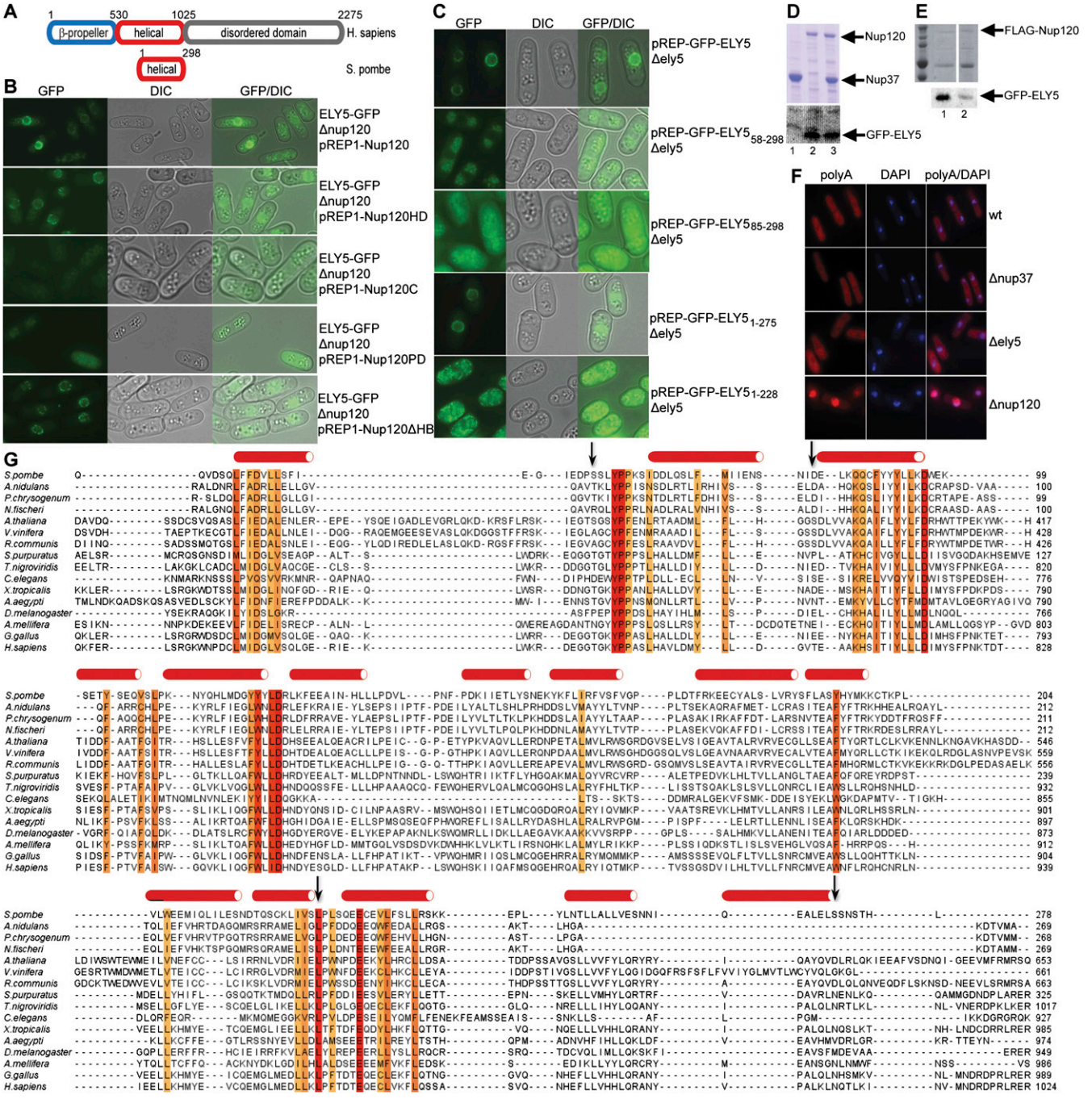

Fig. S1. α-Helical domain of Nup120 targets ELY5 to the nuclear pore. (*A*) Domain structure of *Homo sapiens* ELYS and *S. pombe* ELY5. For human ELYS, β-propeller, α-helical, and C-terminal disordered domains are indicated. *S. pombe* ELY5 contains a α-helical domain (red), which shares similarity with the C-terminal half of the human α-helical domain. (*B*) Expression of Nup120 from a plasmid in Δ*nup120* restores localization of ELY5-GFP (first panel). The α-helical domain, but not the C-terminal end of Nup120, is sufficient for recruiting ELY5 to the nuclear pore complex (NPC) (second and third panels). After complementing the Δ*nup120* strain with the Nup120 β-propeller domain, the characteristic nuclear rim staining of the ELY5-GFP was not observed (fourth panel). Helical bundle insertion in the Nup120 β-propeller domain is not required for correct localization of ELY5-GFP (fifth panel). (Magnification: 1,000×.) DIC, differential interference contrast microscopy. (*C*) Plasmids encoding either full-length *S. pombe* ELY5 or the indicated truncations fused to GFP were transformed into the Δ*ely5* strain. Both full-length ELY5 and $ELY5_{1–272}$ show characteristic nuclear rim staining. Further C-terminal and N-terminal truncations have impaired nuclear pore localization. (Magnification: 1,000×.) (*D*) GFP-ELY5 expressed in *S. pombe* cells was bound to Ni-beads saturated with Nup37 (lane 1), Nup120 (lane 2), or Nup120-Nup37 (lane 3); washed; and eluted. Binding of ELY5 was confirmed via Western blotting using a GFP antibody. (*E*) Affinity purification from *ely5-gfp* (lane 1) and Δ*nup37/ely5-gfp* (lane 2) *S. pombe* strains expressing FLAG-tagged Nup120. Interacting ELY5 was detected using a GFP antibody. (*F*) Strains Δ*nup37* and Δ*ely5* have no mRNA export defect, in contrast to strain Δ*nup120*. (Magnification: 1,000×.) (*G*) Multiple sequence alignment of maximally divergent ELY5 and ELYS sequences within the shared, conserved region. The sequence conservation is colored from white (not conserved) to dark orange (highly conserved). The positions of the *S. pombe* protein truncations are labeled with black arrows. The secondary structure, predicted using PredictProtein, is shown above the sequences. Red cylinders represent α-helical segments.

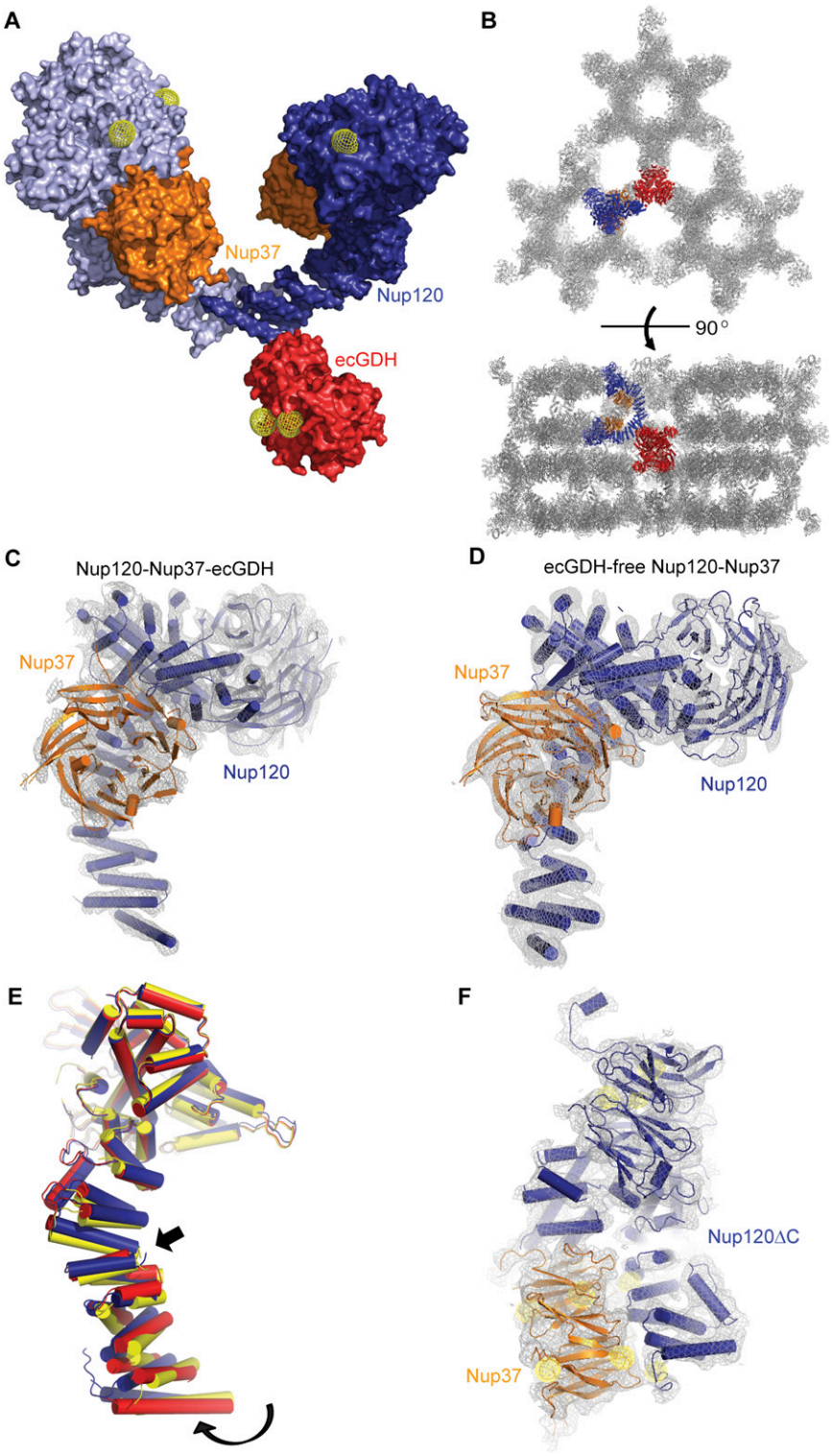

Fig. S2. Crystal packing and phasing of full-length Nup120–Nup37 and Nup120ΔC–Nup37 complex structures. (*A*) Organization of the asymmetrical unit of a crystal with two Nup120-Nup37 heterodimers (Nup120 in blue and Nup37 in orange) and ecGDH (in red). The structure was calculated using combined MR and SAD phases following density modification. The anomalous signal of Ta_6Br_{12} clusters is shown in yellow (anomalous difference density map is contoured at 4.5 σ). (*B*) Copurified ecGDH is positioned on the sixfold crystallographic axis, such that the biologically relevant hexamer (in red) is unambiguously detected after the generation of the crystallographic symmetry equivalents. ecGDH contacts the very C terminus of one Nup120 molecule, and it helps in packing the crystal. The Nup120-Nup37 heterodimer is colored as in *A*. View is rotated 90° horizontally (*Lower*) from the original view (*Upper*). (*C*) Density-modified electron density map of the Nup120-Nup37-ecGDH crystal. The 7.0-Å map is generated by combining $[Ta_6Br_{12}]^{2+}$-single isomorphous replacement (SIR) and MR phases from additional higher resolution structures of unbound Nup37 and ecGDH and is contoured at 1.0 σ. Cocrystallized ecGDH is not shown for simplicity. (*D*) Density-modified electron density map of the ecGDH-free Nup120-Nup37 crystal. The 9.0-Å map is generated by MR phases from the 7.0-Å Nup120–Nup37 complex structure and is contoured at 1.0 σ. (*E*) Superposition of the two Nup120 molecules from the asymmetrical unit of the Nup120-Nup37-ecGDH crystal is

Legend continued on following page

shown in blue and yellow, and the Nup120 molecule from the ecGDH-free Nup120-Nup37 crystal is shown in red. The C-terminal domain can bend vertical to its long axis, which is marked with a curved arrow. The ecGDH does not significantly affect the Nup120 conformation. The straight black arrow indicates where the truncation was made to generate the Nup120ΔC construct. (*F*) Crystals of the Nup120ΔC–Nup37 complex contain one heterodimer in the asymmetrical unit (Nup120 colored in blue and Nup37 colored in orange). The anomalous difference density map, contoured at 4.5 σ, obtained using the Se-SAD signal is shown in yellow.

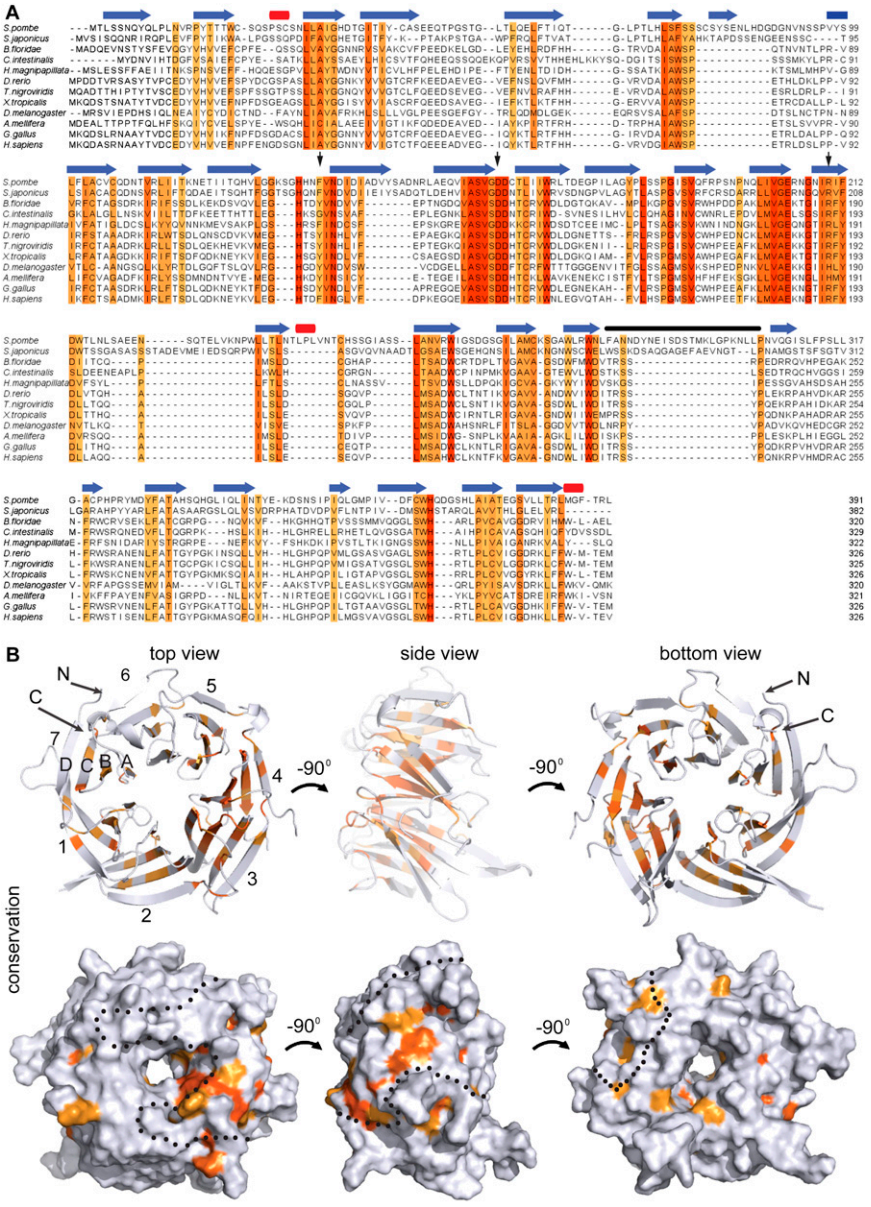

Fig. S3. Multiple sequence alignment of maximally divergent eukaryotic Nup37 sequences. (*A*) Sequence conservation is colored from white (not conserved) to dark orange (highly conserved). The positions of the Nup37 mutations used in this study are labeled with black arrows. The black line marks the position of the loop that we replaced with a serine-glycine loop. The secondary structure is shown above the sequences, with red cylinders representing α-helices and blue arrows representing β-strands. (*B*) Conservation within Nup37 is gradient-colored from gray (not conserved) to dark orange (most conserved). (*Upper*) Majority of conserved residues within Nup37 are structurally important to build the core scaffold. A–D, β-strands; C, C terminus; N, N terminus. (*Lower*) Nup120 binding interface is outlined with a black dotted line on the surface representation of Nup37.

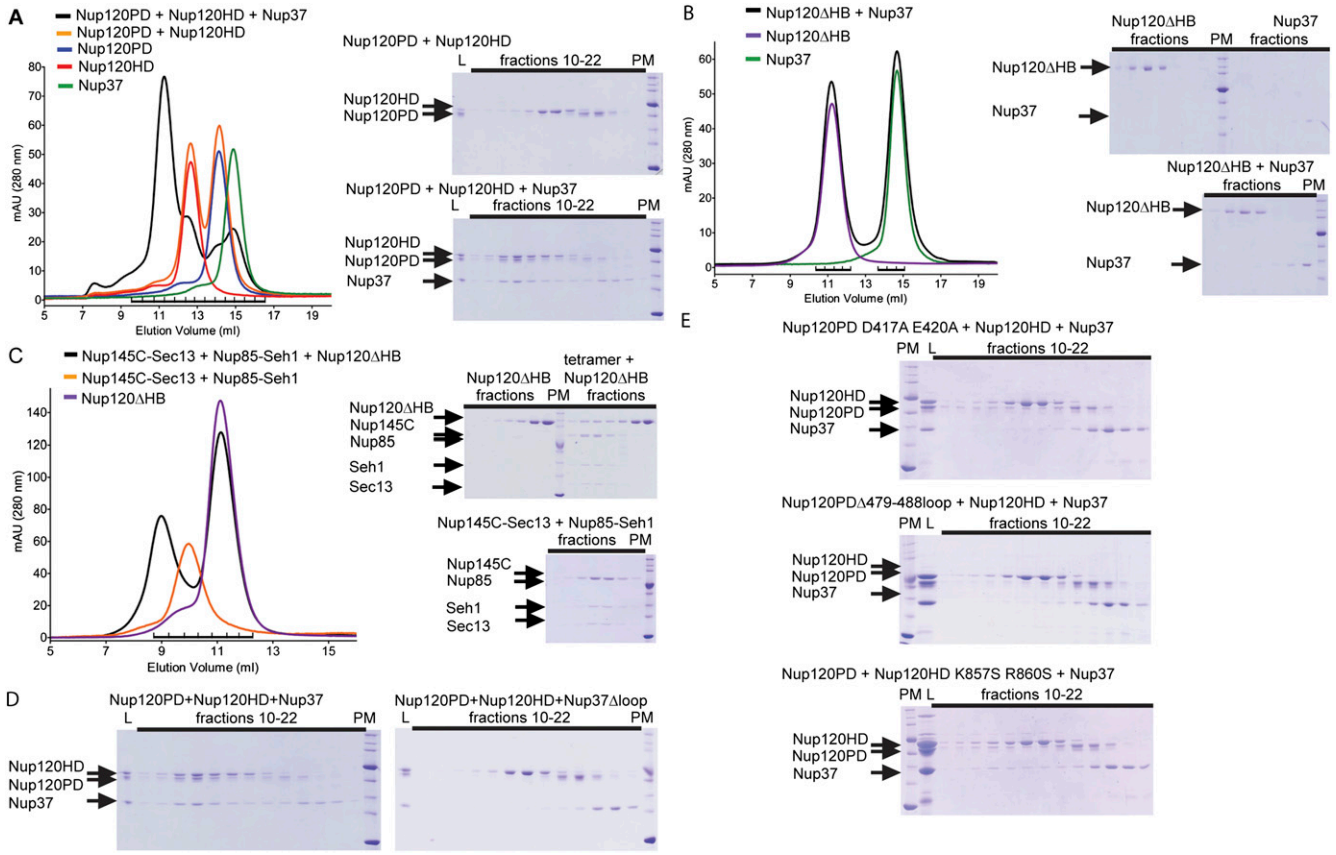

Fig. S4. Nup37 bridges Nup120 subdomains. (*A*) Nup120 α-helical and β-propeller domains do not stably interact, as judged by gel-filtration analysis. However, a mixture of both domains with Nup37 results in a higher molecular-weight species, indicating that Nup37 binds to both domains of Nup120 and stabilizes the interactions between them. Selected fractions, marked with a black bar on the chromatogram, were analyzed by SDS/PAGE. Shown are the loaded proteins (L), 500-μL fractions 10–22 (elution volume: 9.85–16.35 mL), and a protein marker (PM). (*B*) Nup120ΔHB and Nup37 were run separately or as a mixture. Gel-filtration profiles indicate that the α-helical bundle insertion in the β-propeller domain of Nup120 is required for Nup37 binding. Selected fractions, marked with a black bar on the chromatogram, were analyzed by SDS/PAGE. (*C*) Nup120ΔHB is a properly folded protein, as judged by its ability to form a stable complex with the Nup85-Seh1-Nup145C-Sec13 tetramer. SDS/PAGE with the loaded proteins, 500-μL fractions 8–14 (elution volume: 8.85–12.35 mL), and a protein marker is shown. (*D*) Mutations in Nup37 abolish Nup120 binding. Selected gel-filtration fractions, marked with a black bar on the chromatogram in Fig. 4*B*, were analyzed by SDS/PAGE [loaded proteins, 500-μL fractions 10–22 (elution volume: 9.85–16.35 mL), and a protein marker]. Shown are gels with the WT and Nup37Δloop mutant used for binding studies. (*E*) Mutations in the Nup120PD or Nup120HD domain abolish interaction with Nup37. Selected gel-filtration fractions, marked with a black bar on the chromatogram in Fig. 4*E*, were analyzed by SDS/PAGE. Shown are the loaded proteins, 500-μL fractions 10–22 (elution volume: 9.85–16.35 mL), and a protein marker.

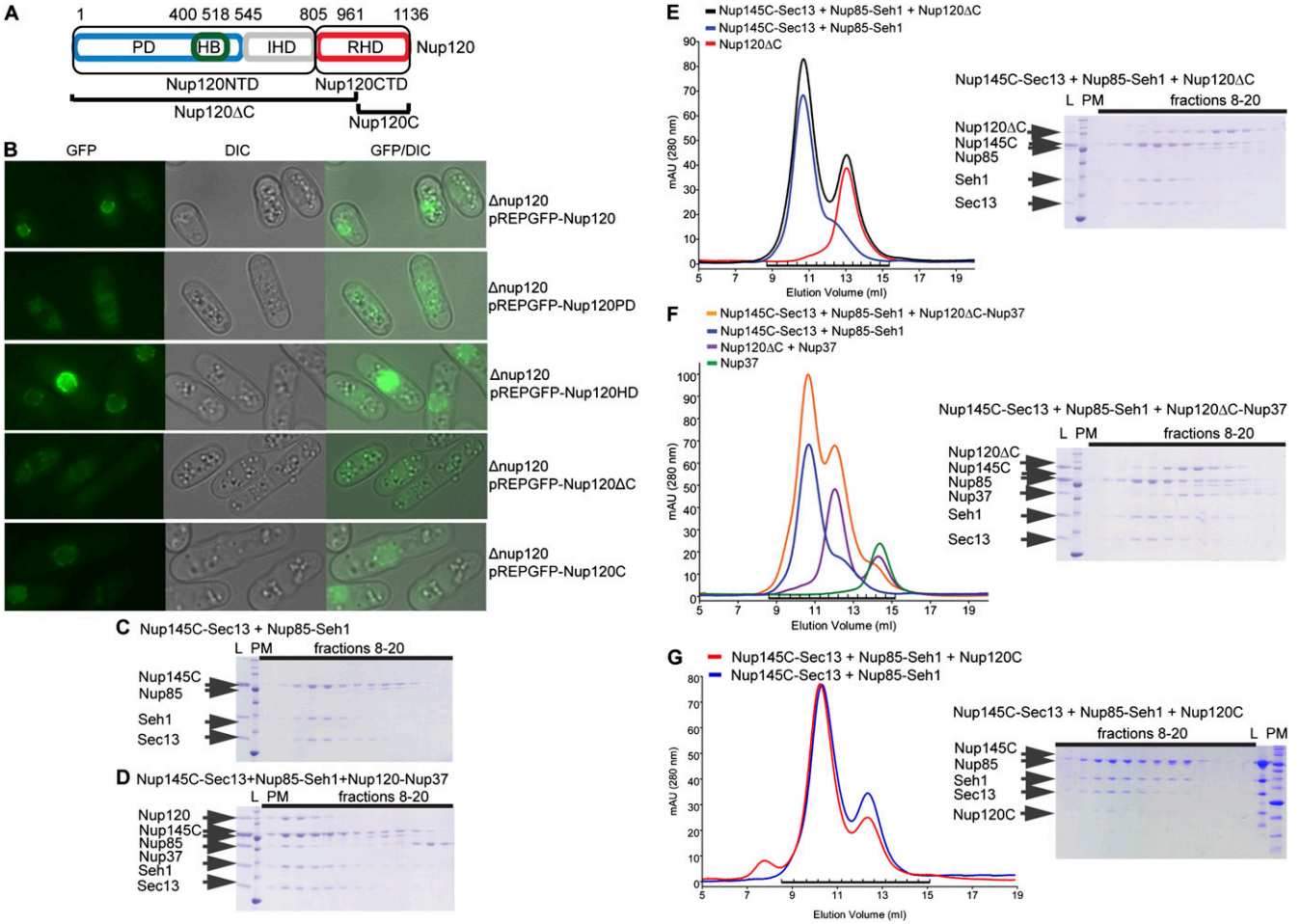

Fig. S5. C-terminal end is sufficient for incorporation of Nup120 into the nuclear pore complex (NPC). (*A*) Domain structure of Nup120 with schematic representation of constructs used for crystallization and biochemical assays. Nup120NTD and Nup120CTD are labeled as in Fig. 2*A*. A shorter Nup120 construct (Nup120ΔC, residues 1–961) used for crystallization is indicated with a black bar, as well as Nup120C (residues 965–1136) used for in vivo experiments. HB, α-helical bundle; IHD, irregular α-helical domain; PD, β-propeller domain; RHD, regular α-helical domain. (*B*) Supplementing the Δ*nup120* strain with plasmid-borne GFP-tagged Nup120 restores the characteristic localization of the protein (first panel). Deletion of the entire α-helical domain or just the last eight α-helices at the C-terminal end of Nup120 abolishes NPC integration (second and fourth panels). Nup120HD, as well as Nup120C, shows correct localization in the Δ*nup120* strain (third and fifth panels). DIC, differential interference contrast microscopy. (Magnification: 1,000×.) (*C*) Formation of the Nup85–Seh1–Nup145C–Sec13 tetrameric complex. Selected gel-filtration fractions, marked with a black bar on the chromatogram in Fig. 5*A*, were analyzed by SDS/PAGE [loaded sample (L), protein marker (PM), and analyzed fractions (elution volume: 8.85–15.35 mL)]. (*D*) Nup37 binds stably to preformed Y-complex. Selected fractions, marked with a black bar on the chromatogram in Fig. 5*B*, were analyzed by SDS/PAGE. Seh1 and Nup37 run at the same position on SDS/PAGE; therefore, SUMO-tagged Nup37 was used to visualize the protein. (*E*) Nup120 without the C-terminal end does not bind to preformed Nup85-Seh1-Nup145C-Sec13 tetramer. Selected fractions, marked with a black bar on the chromatogram, were analyzed by SDS/PAGE. Shown are a loaded sample, protein marker, and analyzed fractions (elution volume: 8.85–15.35 mL). (*F*) Addition of Nup37 does not result in binding of Nup120 to the tetrameric complex if its C-terminal end is missing. Gel-filtration data with fractions analyzed by SDS/PAGE are shown. (*G*) Nup120C forms a stable complex with the Nup85-Seh1-Nup145C-Sec13 tetramer. Binding was analyzed by gel-filtration, and the selected fractions, marked with a black bar on the chromatogram, were analyzed by SDS/PAGE. To detect Nup120C, we used a 15% (wt/vol) SDS/PAGE gel, resulting in Nup85 and Nup145C migrating as a single species.

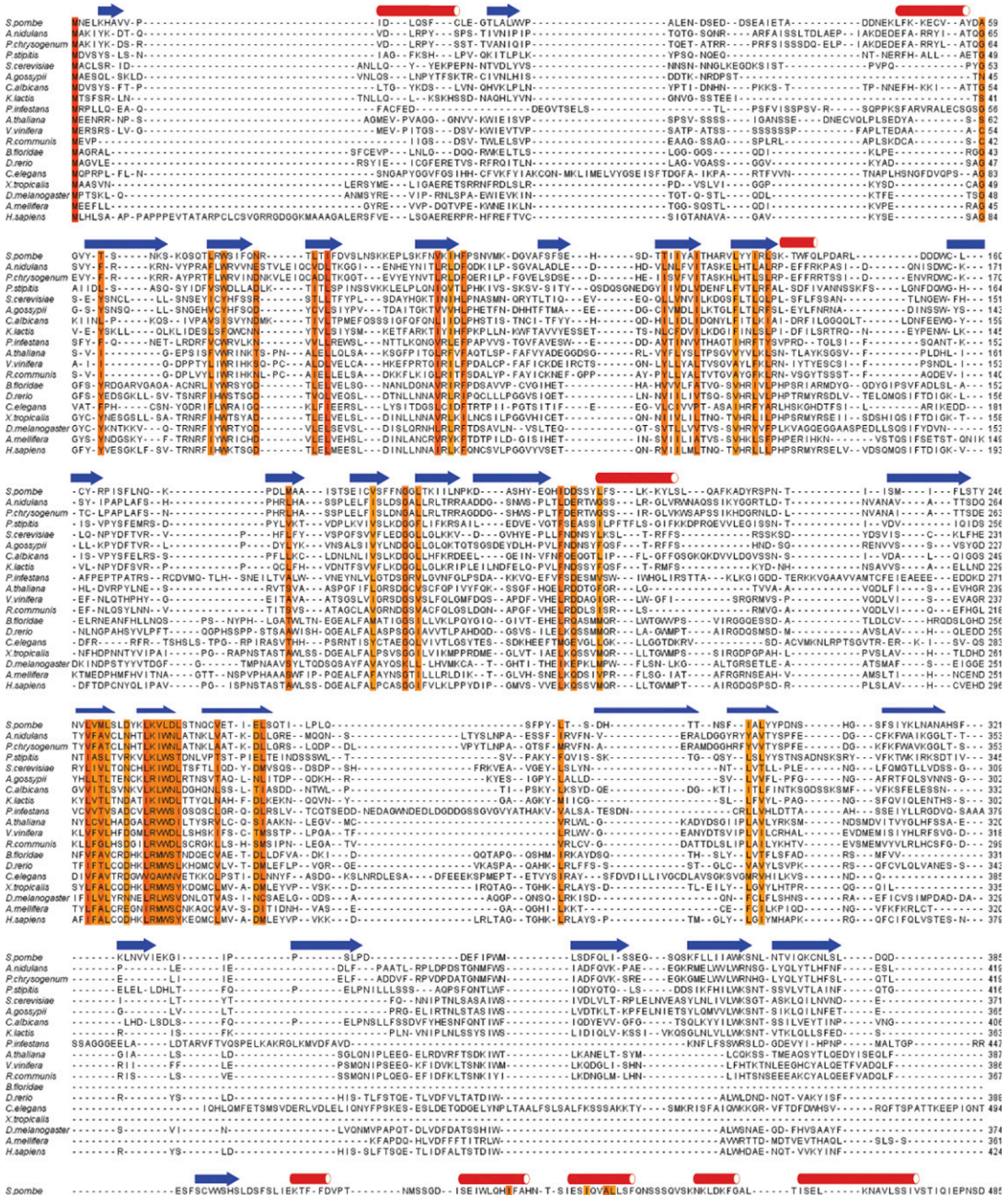

Fig. S6. (Continued)

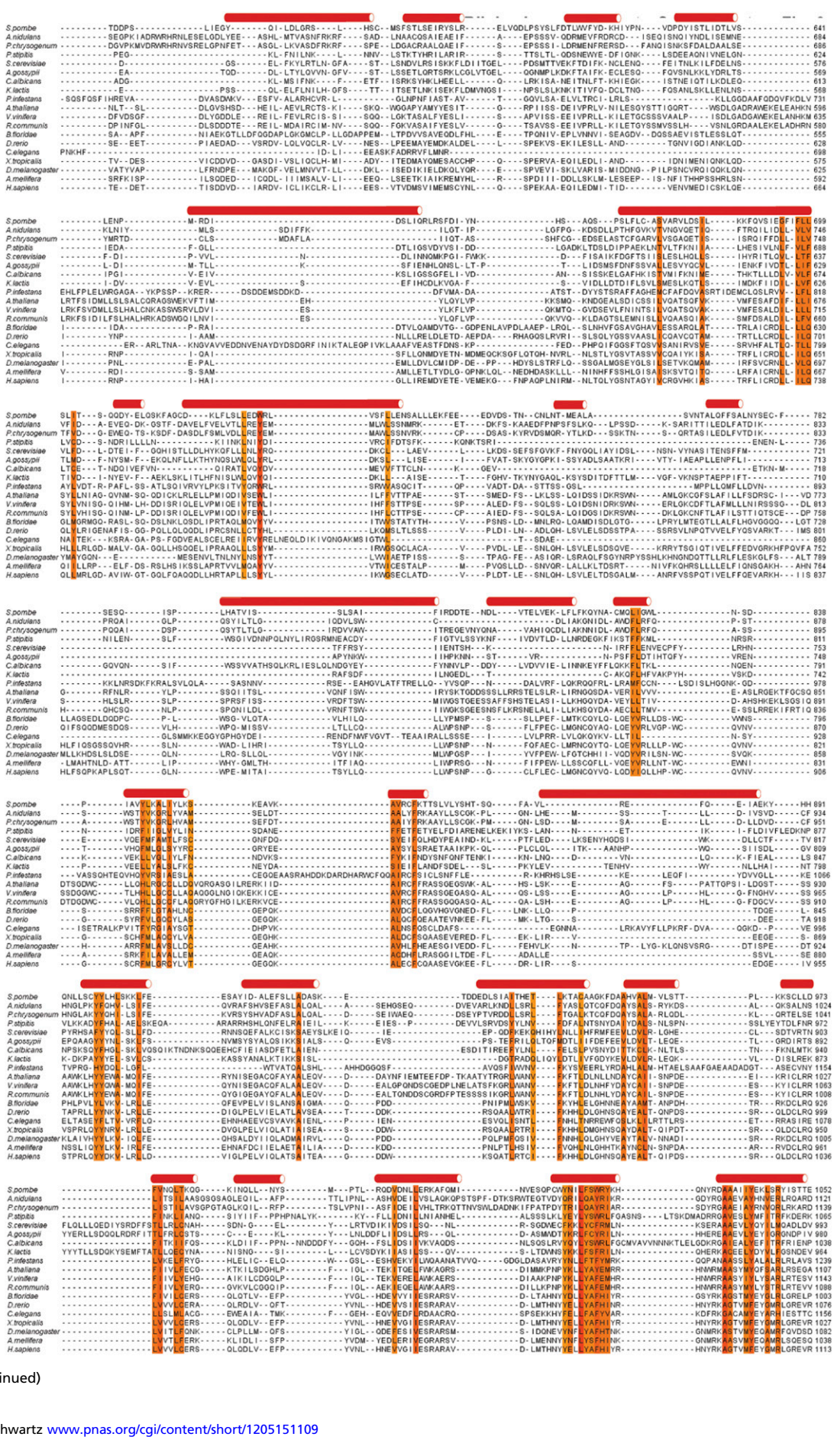

Fig. S6. (Continued)

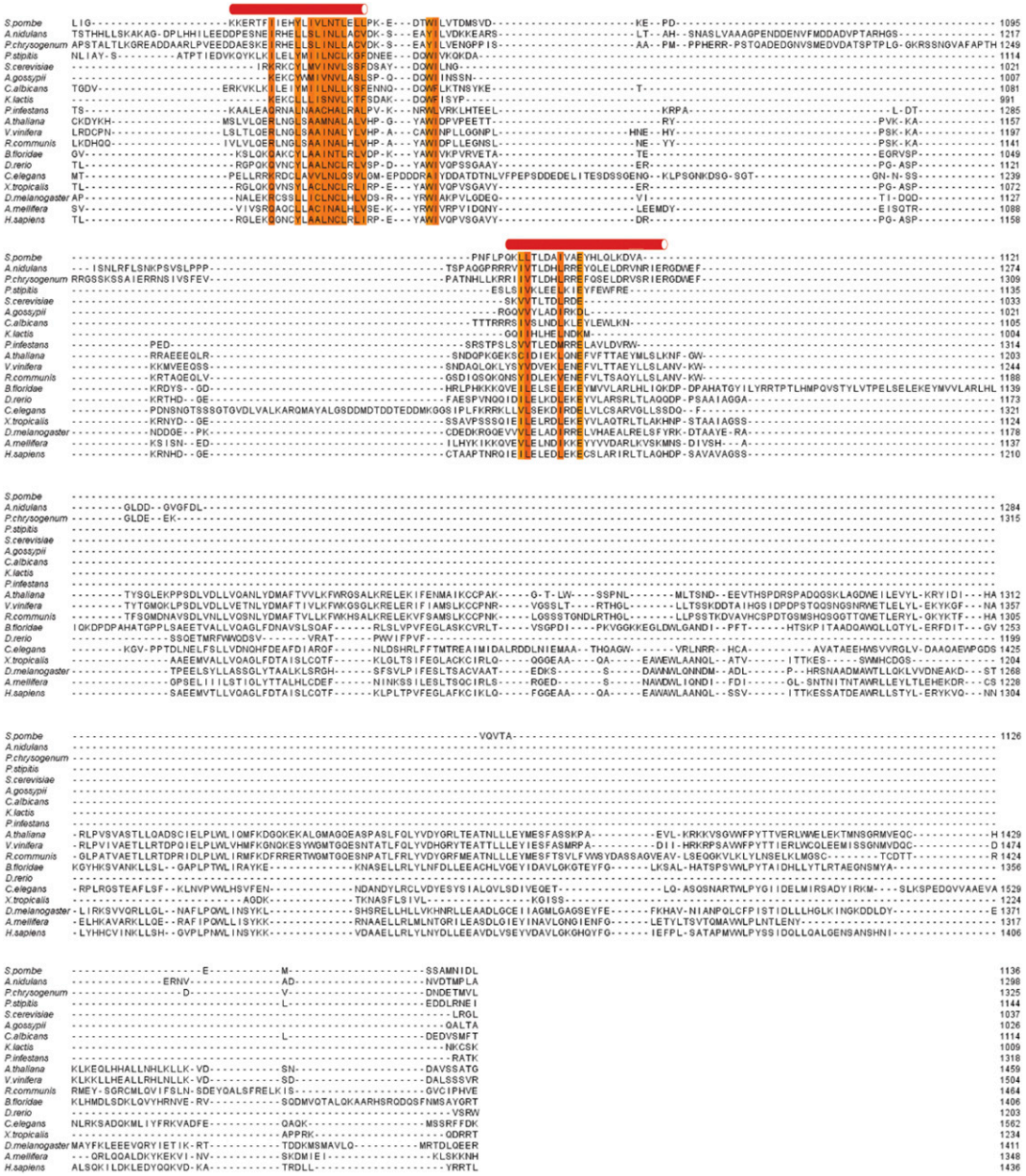

Fig. S6. Multiple sequence alignment of maximally divergent eukaryotic Nup120/160 sequences. The sequence conservation is colored from white (not conserved) to dark orange (highly conserved). Secondary structure elements are shown above the sequences, with blue arrows representing β-strands and red cylinders representing α-helices. PredictProtein was used to predict the secondary structure elements for the region in Nup160 from vertebrates extending beyond the *S. pombe* C terminus.

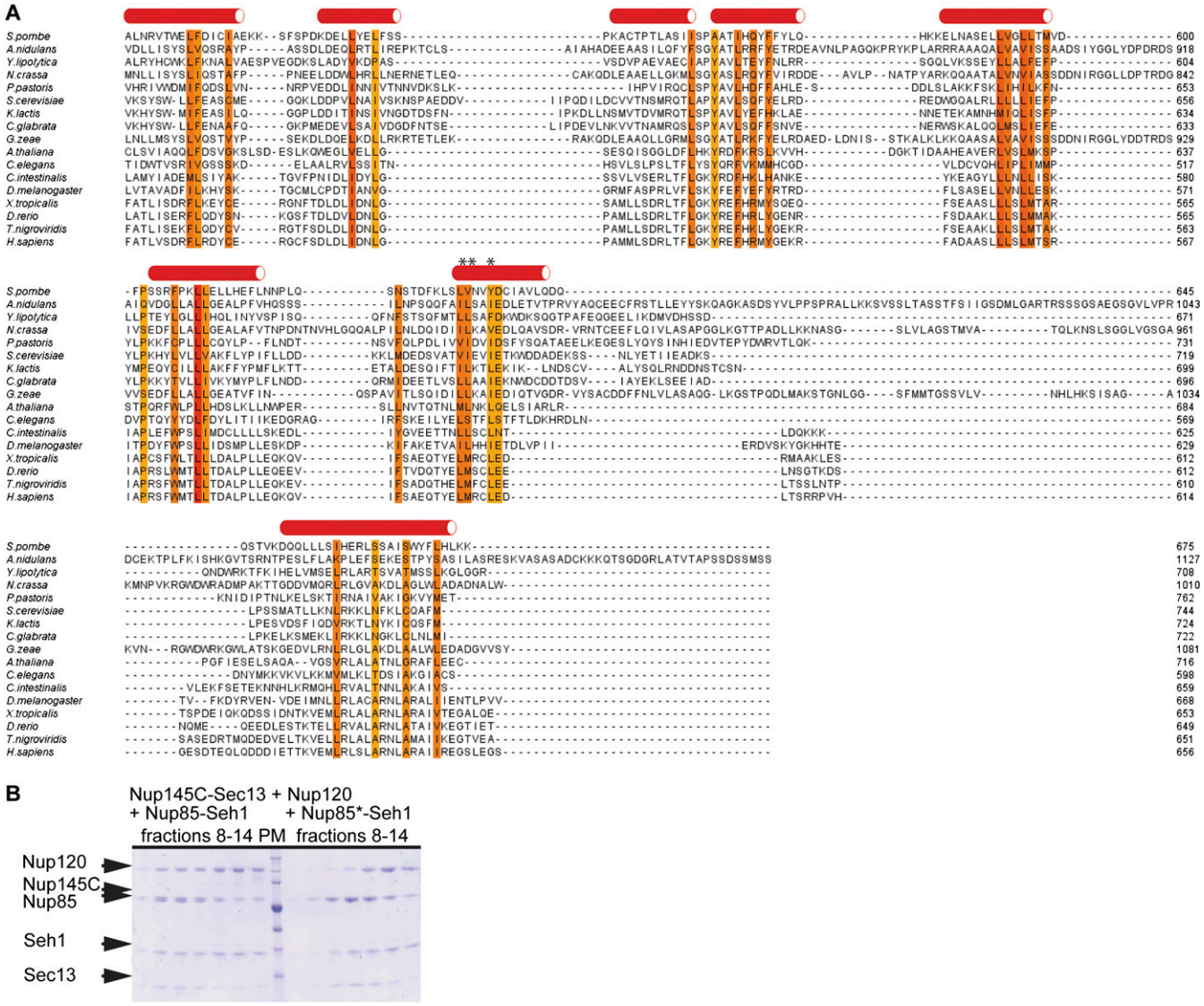

Fig. S7. Tail domain of Nup85 binds Nup120. (*A*) Multiple sequence alignment of maximally divergent eukaryotic Nup85 sequences. Sequence conservation is colored from white (not conserved) to dark orange (highly conserved). PredictProtein was used to predict the secondary structure elements for the tail module of Nup85. The positions of the mutations used in this study are labeled with black stars, whereas red cylinders represent α-helices. (*B*) Selected gel-filtration fractions, marked with a black bar on the chromatogram in Fig. 5*C*, were analyzed by SDS/PAGE. The Nup85–Seh1 complex with mutations in the Nup85 tail module is shown in comparison to a WT complex.

Table S1. Fission yeast strains used in the study

Strain	Genotype
S. pombe	
Δ*nup120*	h^+ *nup120::kanMX leu1-32 de6-210 ura4-D18**
Δ*nup120*	h^- *nup120::kanMX leu1-32 ade6-210 ura4-D18**
Δ*nup37*	h^+ *nup37::kanMX leu1-32 ade6-M216 ura4-D18*
Δ*ely5*	h^+ *ely5::kanMX leu1-32 ade6-M216 ura4-D18*
ELY5-GFP	h^- *ely5-GFP::hph leu1-32 ade6-M216 ura4-D18 his3-Dr*
ELY5-GFP ΔNup37	h^+ *ely5-GFP::hph nup37::kanMX leu1-32 ade6-M216 ura4-D18*
ELY5-GFP ΔNup120	h_+ *ely5-GFP::hph nup120::kanMX leu1-32 ade6-210 ura4-D18*
S. cerevisiae	
L40	*MATa his3-Δ200 trp1-Δ901 leu2-3, 112 ade2 LYS2::(lexAop)4-HIS3 URA3::(lexAop)8-lacZ*

*Provided by V. Doye, Institut Jacques Monod (Paris).

Table S2. Data collection and refinement statistics for native and SeMet-labeled Nup120ΔC–Nup37 complex, as well as native and Ta_6Br_{12}-derivatized full-length Nup120-Nup37 in complex with ecGDH

	Nup120ΔC-Nup37		Nup120-Nup37-ecGDH	
Crystal construct dataset	Native	SeMet	Native	$[Ta_6Br_{12}]^{2+}$
Data collection				
Wavelength, Å	0.9792	0.9792	0.9792	1.2543
Space group	$P4_12_12$	$P4_12_12$	$P6_322$	$P6_322$
Cell dimensions				
a, *b*, *c*; Å	164.1, 164.1, 310.4	164.4, 164.4, 316.3	330.0, 330.0, 349.2	329.7, 329.7, 350.6
Unique reflections	27,671	19,465	18,297	9,391
Resolution, Å	100 to 4.4 (4.5 to 4.4)	100 to 5.0 (5.2 to 5.0)	100 to 7.0 (7.2 to 7.0)	100 to 8.8 (9.1 to 8.8)
R_{pim}, %	6.9 (55.7)	3.8 (27.6)	5.5 (58.8)	4.3 (25.4)
Completeness, %	99.9 (99.9)	99.8 (99.5)	99.5 (95.9)	99.8 (100.0)
Redundancy	11.8 (7.4)	12.9 (10.1)	22.4 (18.8)	11.2 (11.8)
I/σ, I	8.3 (1.5)	12.9 (2.5)	15.2 (1.3)	16.3 (3.6)
Refinement				
Resolution, Å	64.5 to 4.4		100 to 7.0	
No. reflections				
Total	28,523		18,313	
R_{free}	1,452		939	
R_{work}/R_{free}	30.1/34.8		28.5/34.5	
No. atoms	10,113		24,772	
r.m.s.d.				
Bond lengths, Å	0.005		0.006	
Bond angles, °	1.259		1.267	
Ramachandran plot				
Favored/allowed/disallowed, %	87.0/11.3/1.7		91.1/8.0/0.9	

The highest resolution shells with 5% of the data are shown in parentheses. R_{pim}, precision-indicating merging R-factor:

$$R_{pim} = \sum_{hkl}[1/(N-1)]^{1/2}\sum_{i}\left|I_i(hkl) - \overline{I(hkl)}\right| \Big/ \sum\sum_{hkl\ i} I_i\,(hkl)$$

Table S3. Data collection and refinement statistics for native ecGDH

Dataset	ecGDH native
Data collection	
Wavelength, Å	0.9792
Space group	$P2_1$
Cell dimensions	
a, *b*, *c*; Å	105.2, 176.2, 150.2
α,β,γ, °	90, 89.94, 90
Unique reflections	365,923
Resolution, Å	50.0 to 2.0 (2.1 to 2.0)
R_{pim}, %	10.5 (38.1)
Completeness, %	99.2 (92.6)
Redundancy	3.7 (3.2)
I/σ, I	5.1 (1.9)
Wilson B-factor, $Å^2$	24.6
Refinement	
Resolution, Å	50.0 to 2.0
No. of reflections	
Total	364,127
R_{free}	3,646
R_{work}/R_{free}, %	18.2/22.9
No. of atoms	
Protein	40,326
Water	3,833
B-factors, $Å^2$	
Protein	33.4
Water	36.3
r.m.s.d.	
Bond lengths, Å	0.007
Bond angles, °	1.03
Ramachandran plot	
Favored/allowed, %	97.5/2.5

The highest resolution shells with 5% of data are shown in parentheses.
R_{pim}, precision-indicating merging R-factor:

$$R_{pim} = \sum_{hkl}[1/(N-1)]^{1/2}\sum\left|I_i(hkl) - \overline{I(hkl)}\right| \Big/ \sum\sum I_{hkl}\left(\frac{hkl}{i}\right)$$

Table S4. Data collection and refinement statistics for native and SeMet-labeled Nup37 protein

Dataset	Nup37 native	Nup37 SeMet
Data collection		
Wavelength, Å	0.9792	0.9792
Space group	$P4_12_12$	$P4_12_12$
Cell dimensions		
a, *b*, *c*; Å	131.7, 131.7, 117.9	131.7, 131.7, 118.3
Unique reflections	32,471	21,439
Resolution, Å	50 to 2.6 (2.7 to 2.6)	50 to 3.0 (3.1 to 3.0)
R_{pim}, %	3.7 (35.2)	4.2 (28.8)
Completeness, %	100.0 (100.0)	99.9 (99.9)
Redundancy	9.5 (9.6)	14.3 (14.1)
I/σ, I	16.9 (2.7)	18.5 (3.1)
Wilson B-factor, $Å^2$	65.6	
Refinement		
Resolution, Å	50.0 to 2.6	
No. reflections		
Total	31,092	
R_{free}	1,921	
R_{work}/R_{free}, %	17.6/18.9	
No. atoms		
Protein	2,673	
Water	129	
$[SO_4]^{2-}$	5	
B-factors, $Å^2$		
Protein	53.9	
Water	55.7	
$[SO_4]^{2-}$	55.7	
r.m.s.d.		
Bond lengths, Å	0.003	
Bond angles, °	0.834	
Ramachandran plot		
Favored/allowed, %	95.8/4.2	

The highest resolution shells with 5% of the data are shown in parentheses. R_{pim}, precision-indicating merging R-factor:

$$R_{pim} = \sum_{hkl}[1/(N-1)]^{1/2}\sum_{i}\left|I_i(hkl)-\overline{I(hkl)}\right| \Big/ \sum_{hkl}\sum_{i} I_i(hkl)$$

Table S5. Data collection for native Nup120–Nup37 complex

Dataset	Nup120-Nup37 native
Data collection	
Wavelength, Å	1.3776
Space group	$P6_222$
Cell dimensions	
a, b, c; Å	235.0, 235.0, 167.9
Unique reflections	2,256
Resolution, Å	100.0 to 9.0 (9.2 to 9.0)
R_{sym}, %	26.7 (94.3)
Completeness, %	98.9 (97.1)
Redundancy	7.4 (7.7)
I/σ, I	14.2 (3.2)

The highest resolution shells with 5% of the data are shown in parentheses. $R_{sym} = |I_i - I_i|/I_i$, where I_i is the intensity of the ith observation and I_i is the mean intensity of the reflection.

Table S6. MR statistics for native Nup120–Nup37 complex

MR Program	Phaser
Resolution, Å	50.0 to 9.0
RFZ	3.7
TFZ	10

RFZ, rotation function Z-score; TFZ, translation function Z-score.